RSC Advances

This article can be cited before page numbers have been issued, to do this please use: M. SHKIR, S. AlFaify, M. SHABBIR, A. Irfan, P. S. Patil, M. Arora, H. Algarni and J. Zhang, *RSC Adv.*, 2015, DOI: 10.1039/C5RA13494C.

ROYAL SOCIETY OF CHEMISTRY

www.rsc.org/advances

View Article Online
DOI: 10.1039/C5RA13494C

Investigation on the key features of D-π-A type novel chalcone derivative for opto-electronic applications

Mohd. Shkir[a,d], Shabbir Muhammad[a,d*], Salem AlFaify[a,d], Ahmad Irfan[c,d], Parutagouda Shankaragouda Patil[b], Manju Arora[e], Hamid Algarni[a], Zhang Jingping[f]*

[a]*Department of Physics, Faculty of Science, King Khalid University, P.O. Box. 9004 Abha 61413, Saudi Arabia*
[b]*Department of Physics, K. L. E. Institute of Technology, Opposite Airport, Gokul, Hubli 580 030, India*
[c]*Department of Chemistry, Faculty of Science, King Khalid University, Abha 61413, P.O. Box 9004, Saudi Arabia*
[d]*Research Center for Advanced Materials Science (RCAMS), King Khalid University, P.O. Box 9004, Abha 61413, Saudi Arabia.*
[e]*CSIR-National Physical Laboratory, Dr. K.S. Krishnan Road, New Delhi 110012, India*
[f]*Institute of Functional Material Chemistry, Faculty of Chemistry, Northeast Normal University, Renmin Road 5268, Changchun, Jilin 130024, P.R. China*

Abstract

The current work is focused on donor-bridge-acceptor (D-π-A) type novel organic charge transport and nonlinear optical material 1-(4-bromophenyl)-3-(2,4,5-trimethoxyphenyl) prop-2-en-1-one (2,4,5-TMBC) to spotlight its various important properties through experimental and quantum chemical approaches. The compound 2,4,5-TMBC was synthesized by Claisen-Schmidt condensation reaction and its single crystal was grown by slow evaporation solution growth technique. FT-IR and FT-Raman spectra of 2,4,5-TMBC were recorded and investigated. The molecular geometry of 2,4,5-TMBC was optimized by HF, B3LYP, CAM-B3LYP, wb97xd and LC-BLYP methods using 6-31G* basis set. The calculated geometrical parameters and vibrational spectra are in good agreement with the experimental ones. The time dependent density functional theory (TD-DFT) has been applied to investigate the optical properties of the titled compound. The absorption wavelength calculated at TD-B3LYP/6-31G* level of theory in gas phase was found in good covenant with the experimental value (~400nm) as compared with other methods. The HOMO-LUMO energy gap was calculated at all the applied levels of theory. The total dipole moment, polarizability, anisotropy of polarizability and static first and total hyperpolarizability values of 2,4,5-TMBC molecule were calculated at different levels of theory. The dipole moment and first hyperpolarizability values are found to be many folds (2 and 56

View Article Online
DOI: 10.1039/C5RA13494C

times calculated at B3LYP) higher than urea molecule. It is also expected that 2,4,5-TMBC would be electron transport material due to the smaller electron reorganization energy value. The study of nonlinear optical (NLO) properties shows that the 2,4,5-TMBC molecule would be an outstanding candidate for NLO device applications.

Keywords: Chalcones; FT-Raman spectroscopy; Optical properties; nonlinear optical material; Density functional theory

1. Introduction

The chalcones (1, 3-diaryl-2-propen-1-ones) are open chain flavonoids that are extensively biosynthesized in plants. In recent years an extended scientific research on chalcone pageant fascinating biological properties such as anti-ulcer, anti-cancer, antimitotic, anti-inflammatory, anti-malarial, anti-fungal, anti-HIV and antioxidant activities [1-8]. Moreover, the chalcone molecules with a π-conjugated system that provides a large charge transfer axis. The apposite groups of molecules on two aromatic rings act as donors and acceptors [9, 10]. In such molecules the charges can be transferred from donor to acceptor through the charge transfer axis. The resilient intermolecular interactions in any molecule, giving upswing to second harmonic generation (SHG) efficiency [11, 12]. Chalcones are having exceptional optical possessions including high extinction coefficients for absorption in the ultra violet (UV), and noteworthy nonlinear optical (NLO) responses[13-15].

Because of the substantial importance of these compounds, the NLO properties of a series of chalcones have recently been examined experimentally and shown encouraging outcomes in the future application like optical limiters and nonlinear frequency conversion [16-21]. To develop such systems for future device applications, it is important to fathom the fundamental characteristics about their structural and electronic basis of the optical properties.

View Article Online
DOI: 10.1039/C5RA13494C

To explain the structural and electronic properties in an immense class of materials, ranging from atoms and molecules to crystals and complex prolonged structures the density functional theory (DFT) has been proved to be tremendously efficacious and it is also computationally modest. Due to such reasons, DFT has been developed as mutual contrivance in first-principles calculations directed to predict and describe the characteristic properties of molecular and condensed matter schemes. In recognizing the ingredients and providing information about the composition, structure, conformation, functional groups and intra-molecular interactions in new as well as existing complexes; the vibrational spectroscopy has become an excellent tool. DFT provides an irreplaceable spectrum for every definite compound. Many studies have been performed by Hartree-Fock (HF) as well as DFT on various organic, semiorganic, inorganic, chalcones, and their complexes and correlated with experimental reports [22-40].

Recently, Patil et al., had synthesized and grown the bulk single crystals of a new NLO chalcone derivative 1-(4-bromophenyl)-3-(2,4,5-trimethoxyphenyl) prop-2-en-1-one (2,4,5-TMBC), which explores its possible application for NLO devices [41, 42]. This chalcone derivative possesses so-called donor-bridge-acceptor (D-π-A) type structure. The 2,4,5-trimethoxy acts as a donor at one end and 1-(4-bromophenyl)ethanone with C=O bond and the bromo group is an acceptor at the other terminal end of above titled molecule (Fig. 1).

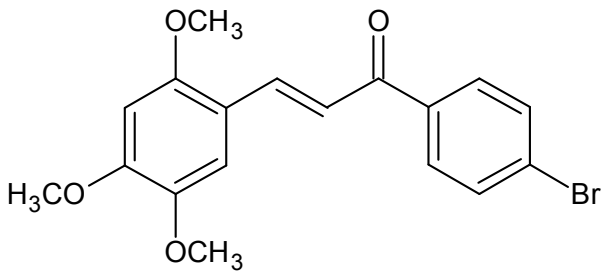

Fig. 1. Chemical structure of 2,4,5-TMBC.

View Article Online
DOI: 10.1039/C5RA13494C

As per the current available literature, no theoretical study has been performed on 2,4,5-TMBC molecule so far, which is necessary to have complete understanding about the compound from various applications point of view.

Therefore, in the current investigation, our aim is to limelight the molecular structural, IR and Raman spectroscopy (experimental and theoretical), electronic, charge transport and nonlinear optical properties of D-π-A type molecule 2,4,5-TMBC. The obtained results have been compared with the experimental data where available.

2. Experimental details

Initially the synthesis of 2,4,5-TMBC achieved by the condensation of 2,4,5-trimethxybenzaldehyde (0.01 mol) with 4-bromoacetophenone (0.01 mol) in 60 ml ethanol in the company of a catalytic amount of sodium hydroxide solution (5 mL, 20%). The continuous stirring was done for more than 2 h and further the substances of the flask were transferred into 500 mL ice-cold water and left to stand for 12 h. The synthesized crude solid was filtered, successively washed with the solution of dilute HCl and distilled water, and then recrystallized it more than twice from acetone to get the pure chalcone. The synthesized 2,4,5-TMBC was further used to grow the single crystals by solution growth technique with slow evaporation at constant temperature. The more details are available in previous report [42].

Fourier Transform Infrared spectra were measured in transmission mode in the range 4000–400 cm^{-1} using a NICOLET 6700 FT-IR spectrometer at ambient temperature. The samples were taken in KBr pellet form. Each spectrum is an average of 32 number of scans at 4 cm^{-1} resolution.

View Article Online
DOI: 10.1039/C5RA13494C

The measurement of Fourier Transform Raman spectra of 2,4,5-TMBC was done on a Nicolet NXR – FT-RAMAN spectrometer in the region 4000–50 cm^{-1} having 1064 nm Nd: YVO4 laser as the excitation source.

3. Computational methodology

The optimized and stable geometry of 2,4,5-TMBC has been achieved by DFT using B3LYP (Becke's three parameter exchange functional B3 combined with Lee-Yang-Parr correlation functional LYP) [43, 44] and Hartree-Fock (HF) at 6-31G* basis set. The visualization of obtained results was performed by Gauss view 5 visualization program [45]. Additional, optimizations of geometries were also done by CAM-B3LYP, wb97xd and LC-BLYP levels of theory. The stability of the optimized geometry was additional confirmed by computing its analytical frequencies. The range-separated functionals are highly dependent on the range-separation parameter. Thus one way to eliminate these ambiguities is to tune the range-separation parameter (especially for donor-acceptor complexes) [46, 47]. Moreover, these techniques could make the theoretical calculations match even closer to experiment. Furthermore, To calculate the structural parameters in the periodic boundary conditions, we have imported the crystal information file (CIF) and optimized it by using generalized gradient approximation GGA/PBE [48] functional and DNP basis set [49]. The DMol3 code [50] which is implemented in the Accelrys package Materials Studio [51] has been used to compute the geometries.

The total first hyperpolarizability (β_{tot}) and its components for 2,4,5-TMBC molecule were evaluated using finite field (FF) approach at all above levels of theory. The FF approach has been widely used to calculate the first hyperpolarizability of numerous chemical systems and it has provided very steady results with experimental data.[52, 53] Here, we have applied various methods including B3LYP, HF, range separated hybrid functional such as CAM-B3LYP and

View Article Online
DOI: 10.1039/C5RA13494C

wb97xd and long range corrected LC-BLYP at 6-31G* basis set for calculating the dipole moment and first hyperpolarizability and compared them with each other. In FF approach, generally a static electric field (F) is applied and the energy (E) is expressed by the following equation:

$$E = E^{(0)} - \mu_1 F_1 - \frac{1}{2}\alpha_{ij}F_iF_j - \frac{1}{6}\beta_{ijk}F_iF_jF_k - \frac{1}{24}\gamma_{ijkl}F_iF_jF_kF_l - \cdots \quad (1)$$

Here $E^{(0)}$ represents the total energy of molecule in the absence of an electronic field, μ is the vector component of the dipole moment, α is the linear polarizability, β and γ are the second and third-order polarizabilities respectively, while x, y and z label the i, j and k components, respectively. It can be seen from Eq.1 that differentiating E with respect to F obtains the μ, α, β, and γ values.

The electronic dipole moment, molecular polarizability, anisotropy of polarizability and molecular static and first total hyperpolarizability were calculated from the following equations.

For a molecule, its dipole moment (μ) is defined as follows:

$$\mu_{tot} = (\mu_x^2 + \mu_y^2 + \mu_z^2)^{\frac{1}{2}} \quad (2)$$

Total polarizability was calculated by:

$$\alpha_{tot} = \frac{1}{3}(\alpha_{xx} + \alpha_{yy} + \alpha_{zz}) \quad (3)$$

Anisotropy of polarizability was calculated by:

$$\Delta\alpha = \frac{1}{\sqrt{2}}\sqrt{\left[(\alpha_{xx} - \alpha_{yy})^2 + (\alpha_{yy} - \alpha_{zz})^2 + (\alpha_{zz} - \alpha_{xx})^2 + 6\alpha_{xz}^2\right]} \quad (4)$$

First hyperpolarizability components of can be evaluated by expression:

$$\beta_i = \beta_{iii} + \sum_{i \neq j}\left[\frac{(\beta_{ijj} + 2\beta_{jii})}{3}\right] \quad (5)$$

View Article Online
DOI: 10.1039/C5RA13494C

Using x, y, z components the resultant of total first hyperpolarizability (β_{tot}) can be calculated by:

$$\beta_{tot} = \sqrt{\left(\beta_x^2 + \beta_y^2 + \beta_z^2\right)} \quad (6)$$

Where β_x, β_y and β_z are:

$\beta_x = (\beta_{xxx} + \beta_{xxy} + \beta_{xyy})$

$\beta_y = (\beta_{yyy} + \beta_{xxz} + \beta_{yyz})$

$\beta_z = (\beta_{xzz} + \beta_{yzz} + \beta_{zzz})$

Hence, the magnitude of total first hyperpolarizability is given by

$$\beta_{tot} = \sqrt{\left[\left(\beta_{xxx} + \beta_{xxy} + \beta_{xyy}\right)^2 + \left(\beta_{yyy} + \beta_{xxz} + \beta_{yyz}\right)^2 + \left(\beta_{xzz} + \beta_{yzz} + \beta_{zzz}\right)^2\right]} \quad (7)$$

Second-order polarizability (β) known as a third rank tensor that can be described by a 3 × 3 × 3 matrix. Due to Kleinman symmetry ($\beta_{xyy} = \beta_{yxy} = \beta_{yyx}$, $\beta_{yyz} = \beta_{yzy} = \beta_{zyy}$,… likewise other permutations also take same value), the 27 components of the 3D matrix can be reduced to 10 components [54]. These components have been calculated using GAUSSIAN 09 [55]. Similarly, time dependent (TD) with B3LYP, HF, range separated hybrid functional CAM-B3LYP, wb97xd and long range corrected LC-BLYP has been used to estimate the transition energies of titled molecule.

The charge transfer rate can be described by Marcus theory via the following equation [56].

$$W = V^2/h(\pi/\lambda k_B T)^{1/2} \exp(-\lambda/4k_B T) \quad (8)$$

where transfer integral (V) and reorganization energy (λ) are the main parameters which determine the self-exchange electron-transfer rates and finally charge mobility. The smaller λ and larger V would lead to the efficient charge transport properties.

There are two types of λ, i.e., inner λ (the molecular geometry relaxation when an electron is added or removed from a molecule) and outer λ (the variations in the surrounding medium due to

View Article Online
DOI: 10.1039/C5RA13494C

polarization effects). Here, we focused on the inner λ which shows the geometric relaxation in the molecules. The inner λ can be divided into two parts: $\lambda_{rel}^{(1)}$ and $\lambda_{rel}^{(2)}$, where $\lambda_{rel}^{(1)}$ and $\lambda_{rel}^{(2)}$ correspond to the geometry relaxation energy of molecule from neutral to charged state, and from charged to neutral state, respectively [57].

$$\lambda = \lambda_{rel}^{(1)} + \lambda_{rel}^{(2)} \quad (9)$$

These terms were calculated from the adiabatic potential energy surfaces [58].

$$\lambda = \lambda_{rel}^{(1)} + \lambda_{rel}^{(2)} = [E^{(1)}(L^{+/-}) - E^{(0)}(L^{+/-})] + [E^{(1)}(L) - E^{(0)}(L)] \quad (10)$$

where $E^{(0)}(L)$, $E^{(0)}(L^{+/-})$ are the ground-state energies of the neutral and charged states, $E^{(1)}(L)$ is the energy of the neutral molecule at the optimized charged geometry and $E^{(1)}(L^{+/-})$ is the energy of the charged state at the geometry of the optimized neutral molecule.

4. Results and discussion

4.1. Molecular Geometry

The optimized stable molecular geometry of 2,4,5-TMBC by B3LYP using 6-31G* basis set has been shown in Fig. 2 (a), further optimization of its geometry was also done by HF, CAM-B3LYP, wb97xd and LC-BLYP levels of theory (see supplementary data). From Fig. 2 (a) and Fig. S1 (b-e) [see supplementary data]. Additionally, we have studied the geometrical parameters of of 2,4,5-TMBC applying the periodic boundary conditions in which calculated geometrical parameters were compared with the experimental crystal structure in solid-state [59, 60]. It can be seen that there is intra-molecular bonding between O(3) and H(20) with bond length 2.332 Å and O(2) and H(20) with bond length 2.434 Å obtained by B3LYP, while these values calculated by HF are found to be 2.363 Å and 2.448 Å, respectively. These are in close covenant with the experimental values 2.360 Å and 2.450 Å, respectively (presented in Table 1) [41]. These geometrical parameters calculated by periodic boundary conditions at PBE/DNP are also found

View Article Online
DOI: 10.1039/C5RA13494C

in reasonable agreement with experimentally reported values (see Table 1 and Fig. S2). The three methoxy group are attached at C(22), C(25) and C(26) in the molecule which are almost coplanar with C(21) and C(27) of benzene ring. Experimentally, its crystal structure is stabilized by intermolecular C12—H12A···O1^{i} and C16— H16B···O1^{i} interactions (code of symmetry is given in Table 1) and these interactions generate a ring of graph-set motif R12 (7). The short Br1···O4 (−3/ 2 + x, 3/2 − y, 1 −z) contact [3.264 (2) Å] also backs to the crystal structure stabilization. The experimentally observed geometry is shown in Fig. 2(b) [41].

All other bond lengths between C-C, C-H, C-Br, C-O etc. are in well agreement with the available literature [16, 61-64]. Table S1 of supporting information shows the values of key geometrical factors including bond lengths, bond angles and dihedral angles of optimized 2,4,5-TMBC molecule at different levels of theory.

Table 1 Experimental and theoretical hydrogen-bond geometry (Å, ^{o}) parameters of 2,4,5-TMBC.

	Exp. [41]			Theoretically calculated (present work)									
				B3LYP		HF		LC-BLYP		wb97xd		PBE (PBC) [b]	
D−H···A	H···A	D···A	Bond Angle	H···A	Bond Angle	H···A	Bond Angle	H···A	Bond Angle	H···A	Bond Angle	H···A	Bond Angle
C9−H9A···O1	2.45	2.799(5)	102	2.434	98.70	2.448	97.27	2.378	98.73	2.444	97.789	2.461	97.94
C9−H9A···O2	2.36	2.720(5)	103	2.332	100.35	2.363	98.36	2.313	99.68	2.354	98.431	2.315	100.20
C12−H12A···O1[a]	2.57	3.470(4)	164										
C16−H16B···O1[a]	2.57	3.303 (5)	133										

[a] Symmetry code: (i) −x +1, y +1 /2, −z 3/ 2, [b] With Periodic boundary conditions (PBC)

View Article Online
DOI: 10.1039/C5RA13494C

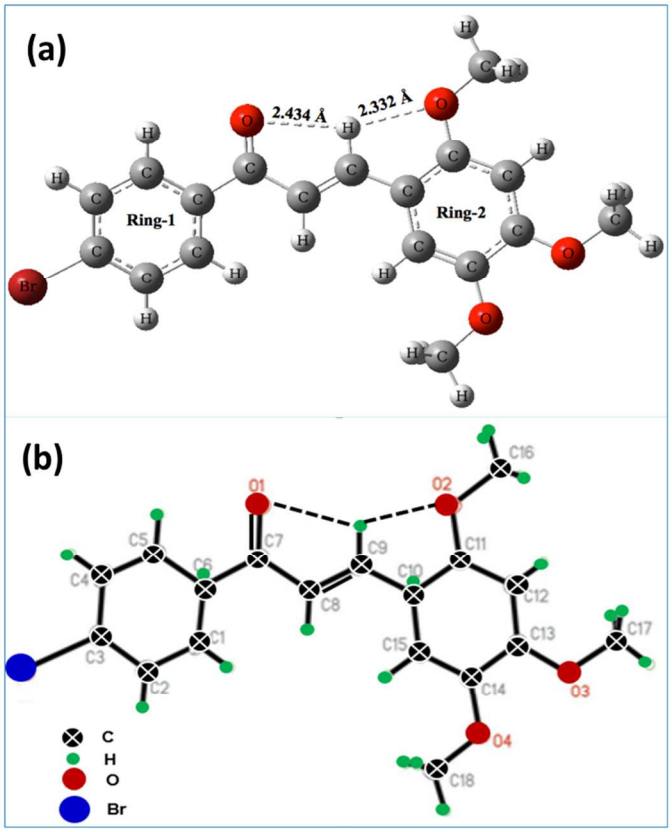

Fig. 2. Optimized molecular geometry of 2,4,5-TMBC molecule (a) B3LYP using 6-31G* basis set and (b) experimentally observed geometry [41].

4.2. Vibrational analysis

Infrared (IR) and Raman spectroscopy techniques have extensively used by the organic chemists for the identification of functional groups, bonding to different molecular conformations and reaction mechanisms by tentatively assigning their observed fundamental modes[65-72]. In vibrational spectroscopy, the shift in peak position is discussed in terms of the change in crystalline field effect induced electronic effects, hydrogen bonding and Fermi resonance Electronic effects arise from back donation and induction of bonded groups present in a material. Inter-molecular and intra-molecular hydrogen bonding appears when H atom and N, O or F atoms are present between two molecules or within a molecule. The vibrational modes in the two phenyl rings will differ in wave number and the magnitude of splitting will depend on the

View Article Online
DOI: 10.1039/C5RA13494C

strength of interactions between different parts (internal coordinates) of the two rings. For some modes, this splitting is too small that they may be considered as quasi-degenerate and for the other modes a remarkable splitting is observed.

1-(4-Bromophenyl)-3-(2,4,5-trimethoxyphenyl) prop-2-en-1-one ($C_{18}H_{17}BrO_4$) possess orthorhombic structure with $P2_12_12_1$ space group and four molecules per unit cell. The unit cell dimensions are a = 7.3031 (3) Å, b = 10.3422 (4) Å, c = 21.3355 (9) Å, V = 1611.47 (11) Å^3 [41, 42].

The orthorhombic crystal system with the non-centrosymmetric space group $P2_12_12_1$ (D_2^4) the Bravais cell consists of 4 molecules and occupy $C_1(4)$ site symmetry. A single molecule of 2,4,5 TMBC contains 40 atoms and 160 atoms in a unit cell. The irreducible representation of the point group where all atoms acquire C_1 site symmetry as:

$$\Gamma total = 120\ A + 120\ B_1 + 120\ B_2 + 120\ B_3$$

which includes the three acoustic modes corresponding to the block translations of the crystal $\Gamma vib, acoustic = B_1 + B_2 + B_3$. The formal classification of fundamental mode predicts that the 456 internal vibrations can be distributed as ($114A + 114B_1 + 114B_2 + 114B_3$) and 24 external modes such as ($3A + 3B_1 + 3B_2 + 3B_3$) translational and ($3A+3B_1+3B_2+3B_3$) rotational vibrational modes. Phonons belonging to B_1, B_2 and B_3 are both Raman and infrared active. The phonons belonging to A symmetry are Raman active and infrared inactive.

The results of factor group analysis and summary are presented in Tables 2 and 3 respectively.

Table 2. Factor group analysis of 2,4,5 TMBC

S. No.	Factor Group Symmetry (D_2^4)	A	B_1	B_2	B_3
1.	External Modes	6	6	6	6
	(i) Translational Modes	3	3	3	3
	(ii) Rotational Modes	3	3	3	3
2.	Internal Modes	114	114	114	114

View Article Online
DOI: 10.1039/C5RA13494C

Table 3. Factor group analysis – summary for 2, 4, 5 TMBC

Factor Group Symmetry (D_2^4)	Site Symmetry External		Internal	C 18	H 17	O 4	Br	Optical Modes	Acoustic Modes
A	3T	3R	114	54	51	12	3	120	0
B_1	3T	3R	114	54	51	12	3	120	1
B_2	3T	3R	114	54	51	12	3	120	1
B_3	3T	3R	114	54	51	12	3	120	1
Total				216	204	48	12	480	3

Internal vibrations

2, 4, 5 TMBC molecule does not have any symmetry and so the internal vibrations exhibited are both IR and Raman active exclusive of acoustic mode. The internal vibrations may be classified as those arising from the CH_2, CH_3, C_6H_5, CH_3O, en-1-one and C-Br functional groups. These vibrations are obtained as a strong bands coupled between themselves.

External vibrations

The external vibrations are generally observed below 500 cm^{-1} due to the rotational and translational modes of vibrations of 2,4,5 TMBC ionic functional groups. The rotational modes are obtained at higher frequency and intensity than translational modes in the Raman spectra. While, the translational modes are more intense in IR spectra.

The theoretical spectra were derived from B3LYP/6-31G* and HF/6-31G* levels of theory. The experimentally recorded and theoretically calculated spectra of 2,4,5-TMBC are shown in Fig. 3. The theoretically prophesied vibrational frequencies have no imaginary frequency, which indicates that the optimized molecular geometry of 2,4,5-TMBC molecule is located at the local minimum point of the potential energy surface. The well-known fact about density functional theory potentials is the overestimation of vibrational wavenumbers. For well comparison with experimental values, the scaling was used for theoretically calculated spectra [for B3LYP it was

View Article Online
DOI: 10.1039/C5RA13494C

0.9613 and for HF it was 0.8929]. The recorded (IR transmittance and Raman) spectra and calculated peak positions of vibrational modes in wavenumber at both B3LYP and HF and their corresponding tentative assignments are listed in Table S2.

IR transmittance and Raman experimental as well as theoretical spectra analysis of 2,4,5-TMBC crystal have been made on the basis of the characteristic vibrations of the methoxy group, carbonyl group, methyl group, phenyl ring with ortho- and para-substitution, bromo-phenyl group and prop-2-en-1-one bridge. The calculated vibrational wavenumber and the atomic displacement corresponding to the different normal modes are used for identifying the ambiguity in vibrational modes. The computed and experimental IR and Raman wavenumbers corresponding to different modes are listed in Table S2 along with detailed assignments. For visual assessment, the experimental and calculated IR transmittance and Raman spectra are presented in Fig. 3. We have tentatively assigned all vibrational bands. The frequencies of the calculated and observed bands are provided in Table S2.

4.2.1. Methoxy (O-CH_3) Group

In methoxy group, CH_3 group is directly attached to oxygen atom, the C-H stretching and bending peak positions can shift either to higher or lower wavenumber depending on the position and electronic effects of groups to which it is bonded in a material [73]. In the present case, three methoxy groups are bonded to phenyl ring at ortho- and para-positions. The asymmetric and symmetric methyl stretching bands are observed as very weak intensity components in the region 2960 – 2850 cm^{-1} at 2952, 2927 cm^{-1} and 2852 cm^{-1} respectively in IR experimental spectrum and at 2952, 2933 and 2844 cm^{-1} in Raman (Exp.) spectrum of this sample [65, 66, 70]. The calculated values of asymmetric and symmetric stretching modes are found at 2929 and 2855 cm^{-1} (B3LYP), 2867 (HF) in IR spectra and at 2965, 2910 (B3LYP), 2925 (HF) cm^{-1} in Raman

View Article Online
DOI: 10.1039/C5RA13494C

spectra respectively. As the calculations were carried out on a free molecule and the experimental spectra were recorded for solid sample, due to intermolecular interactions and crystalline field effects in the sample, the minor variation in peak positions have been observed. This lowering of stretching frequency from the computed values with the decrease in intensity has been explained in terms of the electronic effects caused by back-donation [66] and induced by the oxygen atom [66, 67, 70, 74-76]. The strong asymmetric bending vibration of methyl in methoxy groups appear at 1455, 1558, 1470 cm^{-1} in IR (B3LYP), (HF) and (Exp.) spectra respectively. While, as weak and very weak intensity components in Raman spectra at 1472, 1475 and 1482 cm^{-1} by (B3LYP), (HF) calculated and (Exp.) respectively [77]. The medium intensity band at 1470 cm^{-1} in the IR spectrum has been tentatively assigned to asymmetric bending mode of CH_3 group. The symmetric methyl deformation mode in IR transmittance spectra are at 1381 (B3LYP), 1346 (HF) and 1398 cm^{-1} (Exp.) and in Raman spectra at 1357 (B3LYP), 1346 (HF) and 1394 cm^{-1}. This deformation asymmetric and symmetric modes shifts to higher wavenumber by about 25 cm^{-1} to 50 cm^{-1} as compared to the calculated results (Table S2) is may be due to the electronic effects and strengthening of bonding. The CH_3 rocking vibrations are mixed with C-O stretch and the C-H bending mode, which results a strong peak with a weak band component at 1144 and 1122 cm^{-1} in IR (BL3YP) and as medium intensity band with weak component at 1144 and 1128 cm^{-1} respectively.

4.2.2. Vibrations of phenyl ring

In this 2,4,5-TMBC molecule, the two phenyl rings are bonded to 1 and 3 position of prop-2-en-1-one as 4-Bromophenyl (ring1) and 2,4,5-trimethoxyphenyl (ring2) groups. The benzene ring belongs to D_{6h} symmetry with effective symmetry is C_{2v} or lower due this all twenty vibrations are allowed either in IR or Raman spectroscopy. In these investigations, Herzberg's numbering

View Article Online
DOI: 10.1039/C5RA13494C

system consistent with logical scheme has been adopted as compared to first reported Wilson numbering system applicable for benzene molecule only [71, 72]. The 16 mode of e_{2g} mode of C-C asymmetric stretching vibration modes of two phenyl rings are observed at 1603 (ring1), 1522 (ring2) cm^{-1} (B3LYP), 1617 (ring1), 1532 (ring2) cm^{-1} (HF), 1610 (ring1), 1560 (ring2) cm^{-1} (exp.) in IR transmission spectra and at 1617 (ring1), 1532 (ring2) cm^{-1} (HF) and 1617 (ring1), 1560 (ring2) cm^{-1} (Exp.). While C-C symmetric stretching vibration 13 mode of e_{1u} vibration ~ 1450 cm^{-1} and 9 mode of b_{2u} vibration ~ 1300 cm^{-1} of these two phenyl rings are observed at 1418 (ring1), 1306 (ring2) cm^{-1} (B3LYP), 1403 (ring1), 1303 (ring2) cm^{-1} (HF), 1442 (ring1), 1295 (ring2) cm^{-1} (exp.) in IR transmission spectra and at 1395 (ring1), 1280 (ring2) cm^{-1} (B3LYP), 1403 (ring1), 1276 (ring2) cm^{-1} (HF) and 1455(ring1), 1278 (ring2) cm^{-1} (Exp.) from vibrations of these two modes. The large intensity difference between the two phenyl rings C-C stretching vibrational modes has been attributed to the electronic effects induced by substituting three methoxy and bromo groups in rings. IR transmission spectra exhibits C-H ring stretching modes at 1585 (ring1) (HF), 1587 (ring1) (Exp.) and 1499 (ring2) (B3LYP), 1485 (ring2) (HF), 1511 (ring2) (Exp.) cm^{-1} respectively. While Raman C-H ring stretching modes of ring1 are only observed at 1572 (B3LYP), 1582 (HF), 1575 (Exp.) cm^{-1} and ring2 do not show these modes. The calculated peak values are quite near to the experimental peak positions. The 9 mode of b_{2u} vibration is observed in the IR spectrum at 1327 cm^{-1} and in the Raman spectrum at 1329 cm^{-1} as strong bands. The simultaneous IR and Raman activation of the phenyl ring modes of 16 (e_{2g}), 13 (e_{1u}) and 9 (b_{2u}) provide evidence for the charge transfer interaction between the donor and the acceptor group through the π-system. In tetra-substituted benzene, the C-C-H in-plane bending modes 3(a_{2g}), 17(e_{2g})a, 14(e_{1u})b and 14 (e_{1u})b are found in 1300–1000 cm^{-1} [70] region. The a and b represents higher and lower wavenumber value of e vibrations respectively. The strong band in

View Article Online
DOI: 10.1039/C5RA13494C

IR at 1144 cm^{-1} corresponds to ring mode 14 (e_{1u})b. Mode 17(e_{2g})a is observed as a weak band in Raman spectrum at 1188 cm^{-1}. The increase in intensity of these modes in Exp. spectra has been attributed to the presence of strong electron donor substituent (OCH_3 groups) [65, 66, 70]. The C-C-H out-of-plane bending vibrations is expected to occur in the region around 1000–675 cm^{-1} [66, 70]. The 19(e_{2u})a C-C-H out-of-plane bending vibration is observed as a weak band at 856 cm^{-1} in IR (Exp.) spectrum and 19(e_{2u})b mode is observed at 830 cm^{-1} in the Raman (Exp.) spectrum. The presence of this peak confirms the para-substitution of phenyl ring. The modes corresponding to 11(e_{1g})a are observed as medium intensity and weak band at 742 cm^{-1} and 746 cm^{-1} in IR transmittance (Exp.) and Raman spectrum respectively, which is also in agreement with the theoretical results. In all the aromatic compounds, the carbon–hydrogen stretching vibrations occur in the region 3100–3000 cm^{-1}. The C-H stretching vibrations in the benzene derivatives arise from two non-degenerate modes 1(a_{1g}) at 3081 cm^{-1} IR (exp.), 3083 cm^{-1} Raman (Exp.), 5(b_{1u}) at 3133 cm^{-1} Raman (exp.) and two degenerate vibrations of e_{2g} (3033, 3021 cm^{-1}) in Raman (exp.) spectra, e_{1u} 3041 cm^{-1} (calc.), i.e., the vibrations 1, 5, 15 and 12 modes respectively. A weak band at 3041 cm^{-1} in the Raman spectrum corresponds to the C-H stretching mode 12a. The weak band observed in the IR (Exp.) spectrum at 3081 cm^{-1} corresponds to mode 1(a_{1u} vibration). In benzene, the fundamentals vibrations of a_{1g} (990 cm^{-1}) and b_{1u} (1006 cm^{-1}) are the ring breathing and trigonal bending of 1 and 6 modes, respectively. The trigonal ring bending mode is obtained as a medium intensity band in the IR (exp.) spectrum at 1029 cm^{-1}. The strong IR active ring breathing modes of substituted phenyl rings are observed in the region 795–950 cm^{-1} and tentatively assigned these peaks are listed in Table S2.

4.2.3. Ethylenic bridge vibrations

View Article Online
DOI: 10.1039/C5RA13494C

The vibrations pertaining to ethylenic bridge are very sensitive to the degree of charge transfer between the donor and the acceptor groups, so such stretching modes are important to explore [77]. In 2,4,5 TMBC the C8=C9 stretching mode is observed as a strong band at 1587 cm^{-1} in the IR (Exp.) spectrum and as a strong band at 1575 cm^{-1} in the Raman (Exp.) spectrum, and the corresponding calculated mode is at 1585 cm^{-1} in IR (HF) and at 1572 (B3LYP), 1582 (HF) cm^{-1} in Raman spectra. The strong bands in the Raman spectrum and weak in IR spectrum or vice versa have been attributed to presence or even absence of the inversion symmetry. The intra-molecular charge transfer from the donor to acceptor group through the single-double bond conjugation may induce large variations in the molecular dipole moment and molecular polarizability, hence causing activity in both IR and Raman spectra [74]. So, the simultaneous activation of C8=C9 stretching modes in both IR and Raman spectra confirms the charge transfer interaction between the >C=O group and phenyl ring through the ethylenic bridge. It can be seen from Fig. 3 that the calculated modes at 1585 and 1582 cm^{-1} have strong peaks in both Raman and IR spectrum.

4.2.4. Carbonyl Group Vibration

The wavenumber of the C=O stretch due to carbonyl group mainly depends on the bond strength, which in turn depends upon inductive, conjugative, steric effects and lone pair of electron on oxygen. C=O stretching vibration is expected in the range 1740–1640 cm^{-1}. In the present case very strong C=O experimental band is observed at 1735 cm^{-1} in the IR (Exp.) spectrum and the theoretical value is 1739 cm^{-1} IR (HF) and its conjugation with C=C stretching mode is obtained at 1654 cm^{-1} in IR (Exp.) and 1652 cm^{-1} (Raman (Exp.) spectra. These values are in agreement with reported values [65, 66, 68, 74]. The in-plane and out-of-plane C=O deformations modes are

View Article Online
DOI: 10.1039/C5RA13494C

assigned at 626, 538 cm^{-1} in the IR (Exp.) spectrum and at 537, 500 cm^{-1} in Raman (Exp.) spectrum.

4.2.5. C-Br vibrations

C-Br stretch vibrations are observed below 700 cm^{-1}. In 2,4,5-TMBC crystal, C-Br asymmetric and symmetric stretching modes appear at 707(B3LYP), 667,646 (HF) and 647 (Exp.) cm^{-1} and 448 (B3LYP), 417 (HF) and 437 (Exp.) cm^{-1}, respectively in IR spectra. While in Raman spectra these modes have been observed at 668 (B3LYP), 689 (HF), 703 (Exp.) cm^{-1} and 445 (B3LYP), 453 (HF) and 437 (Exp.) cm^{-1}, respectively. These values are in agreement with the reported values [66, 67, 69-72].

4.2.6. Understanding NLO activity by Vibrational Spectroscopy

The vibrational contribution to Non-Linear Optical (NLO) activity has been characterized by from π-conjugated systems present in a molecule. Such systems have large valued second order molecular polarizabilities which encourages activity of some modes in both IR and Raman spectra. In this case, the simultaneous activity of phenyl ring 16 and 9 modes in IR and Raman spectra have been observed which play crucial role in NLO activity of the crystal. These modes split into 16a, 16b and 9a, 9b peaks. The bands observed in IR (Exp.) at 1587, 1442, and 1324 cm^{-1} are active in the Raman (Exp.) spectrum at 1575, 1455, and 1358 cm^{-1} respectively. The relative intensities of both IR and Raman peaks are comparable due to the electron cloud movement through π-conjugated skeletal structure i.e. from electron donor to electron acceptor group.

View Article Online
DOI: 10.1039/C5RA13494C

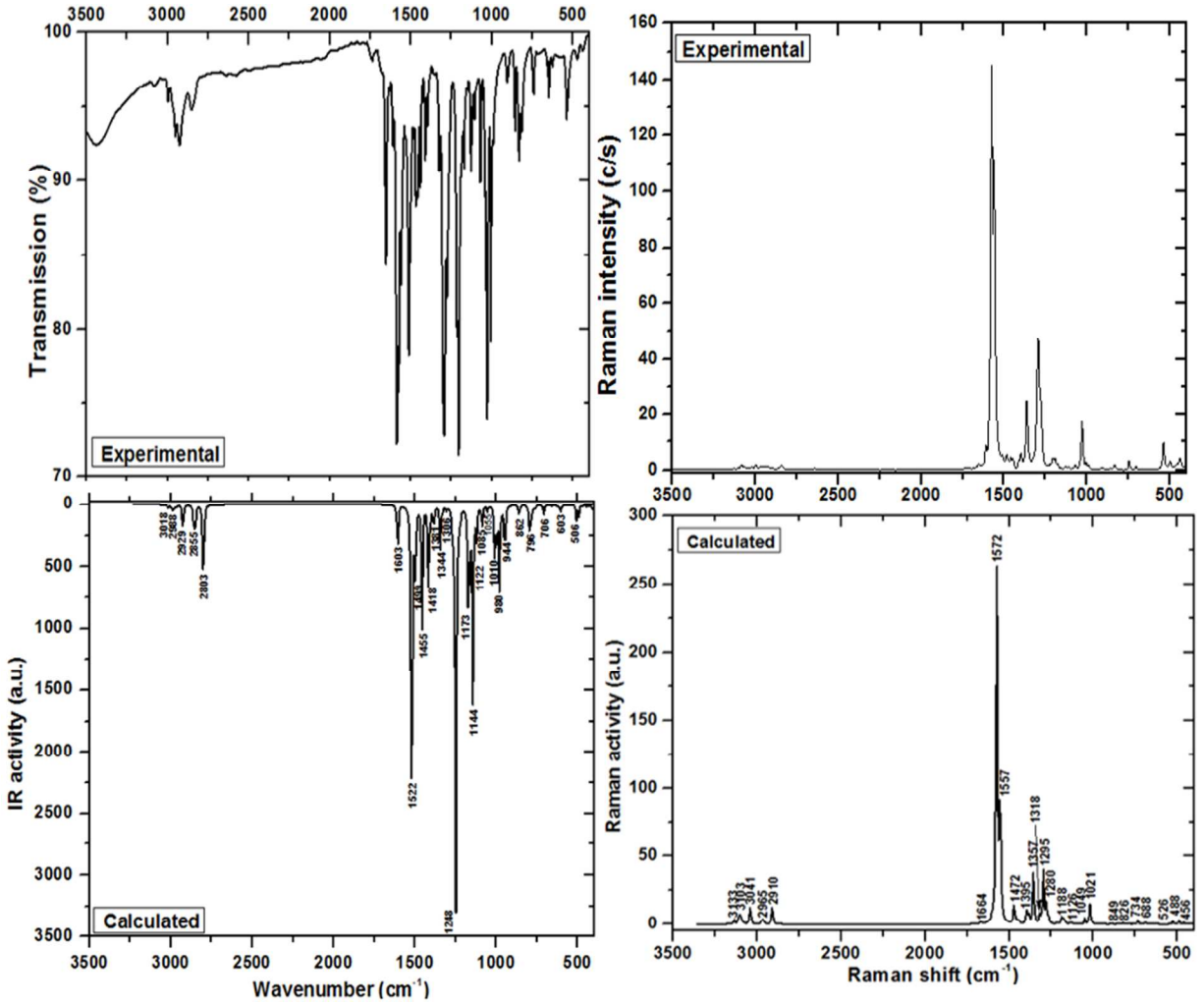

Fig. 3. Calculated and measured (a) IR and (b) Raman spectra of 2,4,5-TMBC**.**

4.3. Electro-optical properties

4.3.1. Frontier Molecular Orbital (FMO) Analysis

In the reactivity of any molecule, frontier molecular orbitals (FMOs) play a vital role. Among FMOs, the interaction of HOMO and LUMO between reacting species is very significant for the progress of chemical reactions in the compound formation through the stabilization of the transition structure of any compound. The HOMO and LUMO energy values were determined at different levels of theory such as B3LYP, HF, CAM-B3LYP, wb97xd and LC-BLYP etc. The values calculated at B3LYP are presented in Table 2. These energy gap values describe the

View Article Online
DOI: 10.1039/C5RA13494C

chemical reactivity, kinetic stability, optical polarizability and chemical softness of any molecule. The molecules with larger HOMO-LUMO energy gaps are known as harder molecules and also possess higher thermal and kinetic stabilities according to softness-hardness rule. The energy gap between HOMO and LUMO of 2,4,5-TMBC molecule is found to be 3.374 eV at B3LYP/6-31G* level of theory with its chemical hardness value of 1.687 eV, indicates that 2,4,5-TMBC molecule has good kinetic stability.

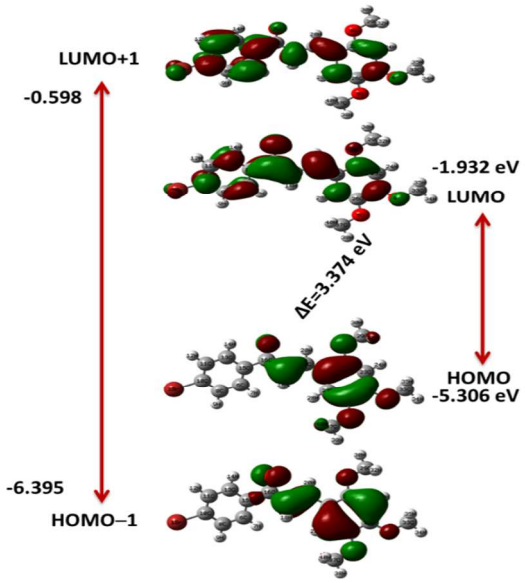

Fig. 4. HOMO and LUMO representation of 2,4,5-TMBC molecule obtained at B3LYP/6-31G* levels of theory.

TD-DFT calculations predict the electronic transition at 3.103 eV (see Table S3 of supporting information) at B3LYP levels of theory corresponding to the transition from ground state to first excited state and show charge transfer from HOMO to LUMO. The 3-D plots of frontier molecular orbitals (FMOs) are shown in Fig. 4 and their respective energy values in eV are given in Table 4.

It can be seen from Fig. 4 that the HOMO are mainly delocalized on one side of the molecule whereas LUMO almost on whole molecule. The electronic density distribution is present on the

View Article Online
DOI: 10.1039/C5RA13494C

whole molecule as indicated by HOMO-LUMO transition and also this transition shows intra-molecular charge transfer in 2,4,5-TMBC molecule. The titled molecule has an advantage of noteworthy transparency and low absorbance as observed experimentally [16, 42] and it is also confirmed by the theoretically calculated value of transition energy which is relatively larger and belongs to violet region of the spectrum. The excitation energy calculated by TDDFT method is found in good correlation with HOMO-LUMO energy gap at same levels of theory i.e. B3LYP.

Table 4 Calculated energy values of frontier molecular orbitals (FMOs) and energy difference of HOMOs and LUMOs in eV at B3LYP/6-31G* levels of theory.

Orbitals	*Energies*
E_{HOMO}	*-5.306*
E_{HOMO-1}	*-6.395*
E_{LUMO}	*-1.932*
E_{LUMO+1}	*-0.598*
$E_{HOMO} - E_{LUMO}$	*3.374*
$E_{HOMO-1} - E_{LUMO+1}$	*5.796*

4.3.2. Time Dependent-Density Functional Theory (TD-DFT) analysis

For excited state electronic structure calculations in quantum chemistry and solid state physics, Time Dependent Density Functional Theory (TD-DFT) establishes itself as one of the most popular theoretical methods. The contemporary density functional approaches show a satisfactory balance between accuracy and computational efficiency when it is compared with the traditional ab initio and semi-empirical approaches. We have applied TD approach at B3LYP, HF, range separated CAM-B3LYP, wb97xd and long range corrected LC-BLYP levels of theory at 6-31G* basis set to examine the nature of electronic transition in 2,4,5-TMBC molecule in gas phase. As per the available literature a precise absorption wavelength at moderately small computing time can be detected easily by such study on the basis of optimized ground state geometry, which corresponds to the vertical electronic transitions in the molecule [78-

View Article Online
DOI: 10.1039/C5RA13494C

[80]. The experimental UV-vis-NIR spectra of 2,4,5-TMBC is already reported in the literature [16, 42]. The absorption wavelength, excitation energies, oscillator strengths, major contributions were calculated in gas phase at the ground state of the optimized geometry and presented in Table S3. The calculated UV-vis spectra (from B3LYP, HF, CAM-B3LYP, wb97xd and LC-BLYP levels of theory) of 2,4,5-TMBC molecule in gas phase are shown in Fig. 5. As clear from Fig. 5 that there is great difference in the value of absorption wavelengths calculated from different methods. We have compared our theoretically calculated absorption wavelength with experimental value, i.e., about 400 nm (recorded spectra is shown in Fig. S3 of supporting information) [42] and found that the value calculated at TD-B3LYP/6-31G* levels of theory (400 nm) is in good agreement in comparison of other applied methods (Table S3). The optimized geometry of 2,4,5-TMBC molecule specifies that the visible absorption maxima of this molecule corresponds to the electron transition from HOMO to LUMO.

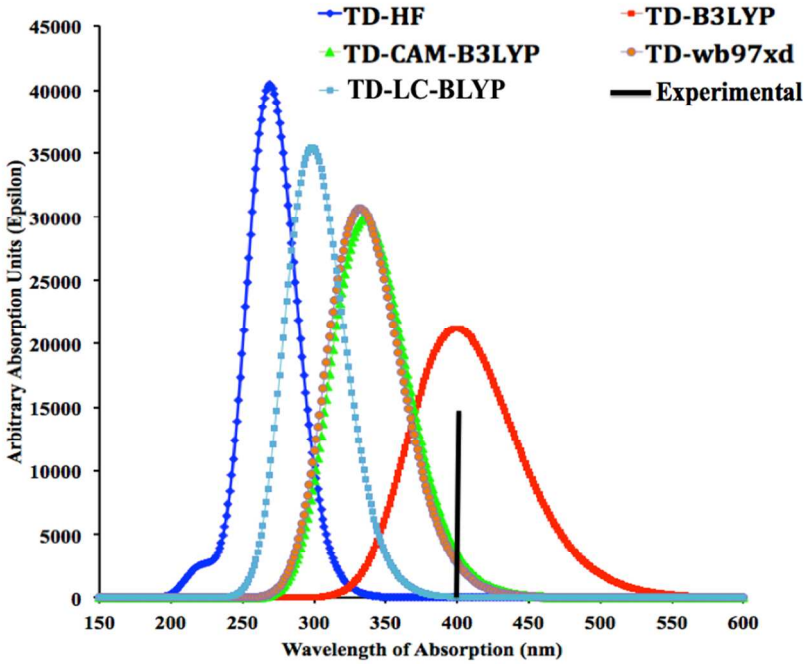

Fig. 5. UV-Visible spectra of 2,4,5-TMBC molecule calculated at different levels of theory using 6-31G* basis set.

View Article Online
DOI: 10.1039/C5RA13494C

4.4. Polarizability and first hyperpolarizability

In nonlinear optical processes of technological importance in device fabrications the hyperpolarizability plays a significant role and vindicates the growing exertion ardent to the precise determination of this property [81, 82]. Several recent studies shows that [83-85] besides an appropriate treatment of electron correlation and a cautious choice of the function basis set, the inclusion of the contributions arising from the nuclear motion is of fundamental importance for the calculations of molecular electrical properties like polarizability and hyperpolarizability. Therefore, we have calculated the electronic total dipole moment (μ_{tot}), molecular total and anisotropy of polarizability (α_{tot}, $\Delta\alpha$), static and total first hyperpolarizability (β_0, β_{tot}) using different methods such as B3LYP, HF, range separated CAM-B3LYP, wb97xd and long range correction LC-BLYP with 6-31G* basis set. The calculated values at B3LYP levels of theory are presented in Table 5 along with 10 components. The values calculated at HF, CAM-B3LYP, wb97xd and LC-BLYP are also presented for comparison in Table S4 (1-4) **(**See supplementary data). Polarizability and hyperpolarizability values are dominated by their diagonal components i.e. components along dipole moment axis of α_{xx} and β_{xxx}. The value of total dipole moment (μ) is 2.343D at B3LYP levels of theory. The variation of hyperpolarizability value at all the applied levels of theory is shown in Fig. S4 along with urea. From figure it is clear that the hyperpolarizability value is found to be higher at B3LYP levels of theory than other methods.

View Article Online
DOI: 10.1039/C5RA13494C

Table 5 Calculated values of polarizability, hyperpolarizability and dipole moment along their individual tensor components of 2,4,5-TMBC molecule at B3LYP/6-31G* levels of theory.

Polarizability and dipole moment			*Hyperpolarizability*		
Components	*a. u.*	*esu* ($\times 10^{-24}$)	*Component*	*a. u.*	*esu* ($\times 10^{-30}$)
α_{xx}	460.421	29.34	β_{xxx}	-4463.056	-38.565
α_{xy}	-0.808	4.30	β_{xxy}	2214.039	19.132
α_{yy}	242.662	36.75	β_{xyy}	-193.007	-1.668
α_{xz}	-6.288	8.00	β_{yyy}	35.940	0.311
α_{yz}	7.913	-4.74	β_{xxz}	96.447	0.833
α_{zz}	99.245	32.90	β_{xyz}	-20.389	-0.176
α_{tot}	315.177	46.699	β_{yyz}	2.185	0.019
$\Delta\alpha$	267.443	39.626	β_{xzz}	39.080	0.338
μ_x	2.257	5.738D	β_{yzz}	8.380	0.072
μ_y	-0.622	-1.582D	β_{zzz}	-5.127	-0.044
μ_z	-0.078	-0.197D	β_0	1467.657	12.682
μ_{tot}	2.343	5.955D	β_{tot}	2446.095	21.137

For α, 1 a. u. = 0.1482×10^{-24} esu, for β, 1 a. u. = 0.008629×10^{-30} esu, μ_{Urea}= 1.3732 D and β_{Urea} = 0.3728×10^{-30} esu [86]

The highest value for μ_x of dipole moment components has been found, which, is a major contributor to the total dipole moment in any molecule. In similar way, the average polarizability (α_{tot}), anisotropy of polarizability (Δα) and total first hyperpolarizability (β_{tot}) of 2,4,5-TMBC molecule have non-zero values of 46.699×10^{-24}, 39.626×10^{-24} and 21.137×10^{-30} esu., respectively. The non-zero value of β_{tot} shows that the titled molecule possesses microscopic first static hyperpolarizability acquired by the algebric second-derivative of the electric dipole moment. The first hyperpolarizability value of 2,4,5-TMBC molecule is 56 times larger than that of urea [β for urea is 0.3728×10^{-30} esu]. The experimental second harmonic generation (SHG) value of 2,4,5-TMBC molecule has been measured and found to be 1.8 times higher than urea [42]. The calculated non-zero β_{tot} and SHG values are many fold higher than organic as well as other reported materials [37-40, 86-93].

View Article Online
DOI: 10.1039/C5RA13494C

4.5. Ionization potentials, electron affinities and reorganization energies

To shed light on the charge transport behavior the ionization potential (IP), electron affinity (EA), λ (h), and λ (e) are significant factors. The smaller/higher IP/EA values means that materials would be efficient hole/electron transporters. The smaller λ (h) and λ (e) revealed proficient hole and electron transport materials, respectively. We have tabulated the IPa, IPv, EAa, EAv, λ (h) and λ (e) in Table 6. The smaller IPa/IPv values of our studied chalcone derivative than 4,6-di(thiophen-2-yl)pyrimidine, i.e., 0.99/0.88 eV, respectively illuminating that prior compound would be proficient hole transport material than later one. [57, 94-96]. The larger EAa/EAv values of chalcone derivative than that of 4,6-di(thiophen-2-yl)pyrimidine, i.e., 0.11/0.7 eV displaying that former would be superior electron transporter as well than the later one. The smaller computed λ (e) of chalcone derivative than the λ (h) illuminating that it would be better electron transport material.

The major alteration from neutral geometry to cation and anion has been found in the C_{15}-C_{16}-C_{17} and C_{17}-C_{19}-C_{21} bond angles. The neutral, cation and anion bond angles in C_{15}-C_{16}-C_{17} (C_{17}-C_{19}-C_{21}) have been observed 118.97^0, 119.07^0 and 119.70^0 (127.90^0, 127.17^0 and 126.88^0), respectively. The key alteration in the geometry has been noticed from neutral to cation, i.e., 0.73^0 and 1.02^0. Thus the geometry relaxation between neutral and cation is greater than anion ensuing more polarization in former one consequently the λ (h) is larger than the λ (e).

Table 6 The vertical and adiabatic ionization potentials (IPv/IPa), vertical and adiabatic electronic affinities (EAv/EAa), hole/electron reorganization energies λ (h)/λ (e) of studied compound at the B3LYP/6-31G* level of theory.

Parameters	IPv	IPa	EAv	EAa	λ (h)	λ (e)
Units	eV	eV	eV	eV	eV	eV
Values	6.80	6.59	0.50	0.65	0.447	0.305

View Article Online
DOI: 10.1039/C5RA13494C

4.6. Global chemical reactivity descriptors (GCRD)

The Global chemical reactivity descriptors (GCRD) parameters are very important to know the connection between structure, stability and global chemical reactivity of molecules and they are based on conceptual DFT. These descriptors are used in the expansion of quantitative structure-activity, structure-property, and structure-toxicity relationships. Hardness of any molecule is related to aromaticity [97]. DFT provides the explanations of principal universal perceptions of molecular structure stability and reactivity [98]. In the current work, we have calculated various GCRD by using E_{HOMO} as ionization potential (I) and E_{LUMO} as electron affinity (A), respectively (Details can be found in supporting information). The computed values of GCRD such as η, μ, S, χ and ω are 1.687, -3.619, 0.733, 3.619 and 1.809 eV, respectively at B3LYP/6-31G* levels of theory. The thermodynamic parameters such as thermal energy (E), specific heat (C_v) and entropy (S) were calculated at HF, B3LYP, CAM-B3LYP, wb97xd and LC-BLYP methods with 6-31G* basis set which have been tabulated in Table S5 (supporting information). The variation of these thermodynamic parameters at different levels of theory is shown in Fig. S5 (supporting information) respectively.

4.7. Molecular Electrostatic Potential (MEP)

The 3-D plot of molecular electrostatic potential (MEP) of 2,4,5-TMBC is theoretically predicted to have better understanding at molecular levels and is shown in Fig. 6. It is the measurement of electrostatic potential on constant electron density surface. The 3-D plots of MEP overlap on the top of total energy density surface. It is a very supportive property to investigate the reactivity of molecular species by predicting that either the approaching nucleophile is attracted towards a positive region of the molecule or the approaching electrophile is attracted towards a negatively charged surface of the molecule. In MEP plot the maximum positive potential (Blue) and

View Article Online
DOI: 10.1039/C5RA13494C

negative potential (red) regions are preferred site for nucleophilic and electrophilic attacks, respectively [38, 39, 99, 100]. The MEP plot of 2,4,5-TMBC is drawn as shown in Fig. 6 to acquire the simultaneous information about its molecular size, shape along with its positive, negative and neutral electrostatic potential regions in terms of color grading.

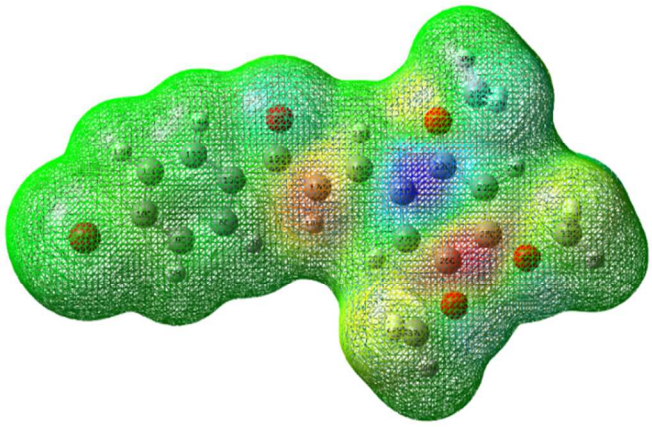

Fig. 6. Molecular electrostatic potential plot of 2,4,5-TMBC molecule with iso value of ±0.02a.u.

5. Conclusion

The ground state molecular geometry of 1-(4-Bromophenyl)-3-(2,4,5-trimethoxyphenyl) prop-2-en-1-one was obtained at DFT and HF methods using 6-31G* basis set. The calculated geometrical parameters at different levels of theory were compared to experimental values and found in good agreement. Furthermore, these geometrical parameters calculated by periodic boundary conditions at PBE/DNP are also found in good agreement with experimentally reported values. Spectral characterization has been done through FT-IR and FT-Raman analysis and found in respectable agreement with the experimental results. The lowering of carbonyl stretching wavenumber indicates the presence of conjugation. The electronic effects of hyperconjugation and back-donation have also been established. The simultaneous IR and Raman activation of the phenyl ring modes of 16, 13 and 9 also provides evidence for the charge

View Article Online
DOI: 10.1039/C5RA13494C

transfer interaction. Hydrogen bonding causes downward wavenumber shifts of peaks. The intermolecular hydrogen bonds give broad bands, while intra-molecular hydrogen bonds produce sharp and well resolved peaks. The comprehensible intra-molecular charge transport has been observed from trimethoxyphenyl moiety (HOMO) to the bromophenyl unit (LUMO). The absorption wavelength determined at TD-B3LYP/6-31G* levels of theory in gas phase was observed at ~ 400 nm which has been found in good agreement with the experimental value of 400 nm. The dipole moment and first hyperpolarizability values are found to be many fold (2 and 56 times calculated at B3LYP) higher than urea molecule. The smaller geometry relaxation from neutral to anion would lead to the smaller electron reorganization energy which ultimately would increase the electron charge transport. The smaller electron reorganization energy than the hole showed that the studied compound might be efficient electron transport material. The calculated MEP plot shows the negative potential sites in the compound by red color, which is favorable for electrophilic attack while the positive potential sites with blue color favorable for nucleophilic attack. The higher value of first hyperpolarizability makes it excellent candidate for fabrication of nonlinear optical (NLO) devices.

Acknowledgements

The authors are thankful to King Khalid University, Abha, Saudi Arabia for providing research infrastructure.

View Article Online
DOI: 10.1039/C5RA13494C

References

1. M. Shigeru, M. Makoto, A. Hironaka and O. Susumu, *Biochemical pharmacology*, 1991, 42, 1447-1451.
2. R. J. Anto, K. Sukumaran, G. Kuttan, M. Rao, V. Subbaraju and R. Kuttan, *Cancer letters*, 1995, 97, 33-37.
3. S. Ducki, R. Forrest, J. A. Hadfield, A. Kendall, N. J. Lawrence, A. T. McGown and D. Rennison, *Bioorganic & medicinal chemistry letters*, 1998, 8, 1051-1056.
4. F. Herencia, M. L. Ferrandiz, A. Ubeda, J. Domínguez, J. E. Charris, G. M. Lobo and M. J. Alcaraz, *Bioorganic & medicinal chemistry letters*, 1998, 8, 1169-1174.
5. M. Liu, P. Wilairat and M.-L. Go, *Journal of Medicinal Chemistry*, 2001, 44, 4443-4452.
6. S. N. López, M. V. Castelli, S. A. Zacchino, J. N. Domínguez, G. Lobo, J. Charris-Charris, J. C. Cortés, J. C. Ribas, C. Devia and A. M. Rodríguez, *Bioorganic & medicinal chemistry*, 2001, 9, 1999-2013.
7. J.-H. Wu, X.-H. Wang, Y.-H. Yi and K.-H. Lee, *Bioorganic & medicinal chemistry letters*, 2003, 13, 1813-1815.
8. L. Mathiesen, K. E. Malterud and R. B. Sund, *Planta medica*, 1995, 61, 515-518.
9. B. Zhao, W.-Q. Lu, Z.-H. Zhou and Y. Wu, *Journal of Materials Chemistry*, 2000, 10, 1513-1517.
10. X. Tao, T. Watanabe, K. Kono, T. Deguchi, M. Nakayama and S. Miyata, *Chemistry of materials*, 1996, 8, 1326-1332.
11. V. Ramkumar, S. Anandhi, P. Kannan and R. Gopalakrishnan, *RSC Advances*, 2015, 5, 586-596.
12. V. Ramkumar, S. Anandhi, P. Kannan and R. Gopalakrishnan, *CrystEngComm*, 2013, 15, 2438-2449.
13. M. Cockerham, C. Frazier, S. Guha and E. Chauchard, *Applied Physics B*, 1991, 53, 275-278.
14. P. Patil, V. Bhumannavar, M. Bannur, H. N. Kulkarni and G. Bhagavannarayana, 2013.
15. R. Nithya, N. Santhanamoorthi, P. Kolandaivel and K. Senthilkumar, *The Journal of Physical Chemistry A*, 2011, 115, 6594-6602.
16. P. Patil, S. Dharmaprakash, K. Ramakrishna, H.-K. Fun, R. S. S. Kumar and D. N. Rao, *Journal of crystal growth*, 2007, 303, 520-524.
17. B. Gu, W. Ji, X.-Q. Huang, P. Patil and S. Dharmaprakash, *Optics express*, 2009, 17, 1126-1135.
18. L. M. Saleh, H. A. Hassan, F. Z. Henari, P. Patil and M. Bannur, *Applied Physics A*, 2014, 116, 805-810.
19. J. Chen, X. Wang, Q. Ren, P. Patil, T. Li, H. Yang, J. Zhang, G. Li and L. Zhu, *Applied Physics A*, 2011, 105, 723-731.
20. B. Gu, W. Ji, P. Patil and S. Dharmaprakash, *Journal of Applied Physics*, 2008, 103, 103511-103511-103516.
21. A. J. Kiran, H. Lee, H. Ravindra, S. Dharmaprakash, K. Kim, H. Lim and F. Rotermund, *Current Applied Physics*, 2010, 10, 1290-1296.
22. T. Vijayakumar, I. H. Joe, C. R. Nair and V. Jayakumar, *Chem. Phys.*, 2008, 343, 83-99.
23. D. Sajan, J. Binoy, I. Hubert Joe, V. Jayakumar and J. Zaleski, *Journal of Raman Spectroscopy*, 2005, 36, 221-236.
24. J. Binoy, I. H. Joe and V. Jayakumar, *Journal of Raman Spectroscopy*, 2005, 36, 1091-1100.
25. D. Sajan, I. H. Joe and V. Jayakumar, *Journal of Raman Spectroscopy*, 2006, 37, 508-519.
26. S. Guidara, H. Feki and Y. Abid, *Spectrochimica Acta Part A: Molecular and Biomolecular Spectroscopy*, 2013, 115, 437-444.
27. N. Elleuch, W. Amamou, A. B. Ahmed, Y. Abid and H. Feki, *Spectrochimica Acta Part A: Molecular and Biomolecular Spectroscopy*, 2014, 128, 781-789.
28. B. G. Johnson, P. M. Gill and J. A. Pople, *The Journal of chemical physics*, 1993, 98, 5612-5626.

View Article Online
DOI: 10.1039/C5RA13494C

29. S. Elleuch, H. Feki and Y. Abid, *Spectrochimica Acta Part A: Molecular and Biomolecular Spectroscopy*, 2007, 68, 942-947.
30. M. Shkir and H. Abbas, *Spectrochimica Acta Part A: Molecular and Biomolecular Spectroscopy*, 2014, 125, 453-457.
31. N. Sudharsana, S. Muthunatesan, G. J. Priya, V. Krishnakumar and R. Nagalakshmi, *Spectrochimica Acta Part A: Molecular and Biomolecular Spectroscopy*, 2014, 121, 53-62.
32. A. Reshak and W. Khan, *J. Alloys Compd.*, 2014, 592, 92-99.
33. S. Azhagiri, S. Jayakumar, S. Gunasekaran and S. Srinivasan, *Spectrochimica Acta Part A: Molecular and Biomolecular Spectroscopy*, 2014, 124, 199-202.
34. M. Shkir and H. Abbas, *Spectrochimica Acta Part A: Molecular and Biomolecular Spectroscopy*, 2014, 118, 172-176.
35. M. Shkir, S. Muhammad, S. AlFaify, A. Irfan and I. Yahia, *Spectrochimica Acta Part A: Molecular and Biomolecular Spectroscopy*, 2015, 137, 432-441.
36. A. Kumar, V. Deval, P. Tandon, A. Gupta and E. D. D'silva, *Spectrochimica Acta Part A: Molecular and Biomolecular Spectroscopy*, 2014, 130, 41-53.
37. M. Shkir, H. Abbas, S. Kumar, G. Bhagavannarayana and S. AlFaify, *J. Phys. Chem. Solids*, 2014, 75, 959-965.
38. M. Shkir, S. AlFaify, H. Abbas and G. Bhagavannarayana, *Mater. Chem. Phys.*, 2015.
39. M. Shkir, S. Muhammad and S. AlFaify, *Spectrochimica Acta Part A: Molecular and Biomolecular Spectroscopy*, 2015.
40. H. Abbas, M. Shkir and S. AlFaify, *Arabian Journal of Chemistry*, DOI: http://dx.doi.org/10.1016/j.arabjc.2015.02.011.
41. P. Patil, M. M. Rosli, H.-K. Fun, I. A. Razak and S. Dharmaprakash, *Acta Crystallographica Section E: Structure Reports Online*, 2006, 62, o4644-o4645.
42. P. Patil, M. Bannur, D. Badigannavar and S. Dharmaprakash, *Optics & Laser Technology*, 2014, 55, 37-41.
43. C. Lee, W. Yang and R. G. Parr, *Phys. Rev. B*, 1988, 37, 785-789.
44. A. D. Becke, *The Journal of Chemical Physics*, 1993, 98, 5648-5652.
45. R. Dennington, T. Keith and J. Millam, *Semichem Inc., Shawnee Mission, KS*, 2009.
46. T. Stein, L. Kronik and R. Baer, *J. Chem. Phys.*, 2009, 131, 244119.
47. B. M. Wong and J. G. Cordaro, *J. Chem. Phys.*, 2008, 129, 214703.
48. J. P. Perdew, K. Burke and M. Ernzerhof, *Phys. Rev. Lett.*, 1996, 77, 3865-3868.
49. A. B. Nadykto, A. Al Natsheh, F. Yu, K. V. Mikkelsen and J. Herb, in *Adv. Quantum Chem.*, eds. E. G. Michael and S. J. Matthew, Academic Press, 2008, vol. Volume 55, pp. 449-478.
50. B. Delley, *J. Chem. Phys.*, 2000, 113, 7756-7764.
51. R. A. I. Materials Studio Modeling, San Diego,, 2004.
52. S. Muhammad, A. Irfan, M. Shkir, A. R. Chaudhry, A. Kalam, S. AlFaify, A. G. Al-Sehemi, A. Al-Salami, I. Yahia and H. L. Xu, *J. Comput. Chem.*, 2015, 36, 118-128.
53. S. Muhammad, H. Xu, M. R. S. A. Janjua, Z. Su and M. Nadeem, *PCCP*, 2010, 12, 4791-4799.
54. D. Kleinman, *Physical Review*, 1962, 126, 1977.
55. M. J. Frisch, G. W. Trucks, H. B. Schlegel, G. E. Scuseria, M. A. Robb, J. R. Cheeseman, G. Scalmani, V. Barone, B. Mennucci, G. A. Petersson, H. Nakatsuji, M. Caricato, X. Li, H. P. Hratchian, A. F. Izmaylov, J. Bloino, G. Zheng, J. L. Sonnenberg, M. Hada, M. Ehara, K. Toyota, R. Fukuda, J. Hasegawa, M. Ishida, T. Nakajima, Y. Honda, O. Kitao, H. Nakai, T. Vreven, J. A. Montgomery, J. E. Peralta, F. Ogliaro, M. Bearpark, J. J. Heyd, E. Brothers, K. N. Kudin, V. N. Staroverov, R. Kobayashi, J. Normand, K. Raghavachari, A. Rendell, J. C. Burant, S. S. Iyengar, J. Tomasi, M. Cossi, N. Rega, J. M. Millam, M. Klene, J. E. Knox, J. B. Cross, V. Bakken, C. Adamo, J. Jaramillo, R. Gomperts, R. E. Stratmann, O. Yazyev, A. J. Austin, R. Cammi, C. Pomelli, J. W.

View Article Online
DOI: 10.1039/C5RA13494C

Ochterski, R. L. Martin, K. Morokuma, V. G. Zakrzewski, G. A. Voth, P. Salvador, J. J. Dannenberg, S. Dapprich, A. D. Daniels, Farkas, J. B. Foresman, J. V. Ortiz, J. Cioslowski and D. J. Fox, Wallingford CT, 2009, DOI: citeulike-article-id:9096580.

56. R. A. Marcus and N. Sutin, *Biochim. Biophys. Acta - Rev. Bioenerg.*, 1985, 811, 265-322.
57. A. Irfan, *Comp. Mater. Sci.*, 2014, 81, 488-492.
58. J. L. Brédas, J. P. Calbert, D. A. da Silva Filho and J. Cornil, *Proceedings of the National Academy of Sciences*, 2002, 99, 5804-5809.
59. A. Irfan, A. G. Al-Sehemi, S. Muhammad, A. R. Chaudhry, A. Kalam, M. Shkir, A. E. Al-Salami and A. M. Asiri, *J. Saudi. Chem. Soc.*, doi:10.1016/j.jscs.2014.12.009.
60. A. G. Al-Sehemi, A. Irfan and A. M. Asiri, *Chin. Chem. Lett.*, 2014, 25, 609-612.
61. F. H. Allen, O. Kennard, D. G. Watson, L. Brammer, A. G. Orpen and R. Taylor, *J. Chem. Soc., Perkin Trans. 2*, 1987, S1-S19.
62. P. Patil, J.-J. Teh, H.-K. Fun, I. A. Razak and S. Dharmaprakash, *Acta Crystallographica Section E: Structure Reports Online*, 2006, 62, o3096-o3098.
63. P. Patil, J.-J. Teh, H.-K. Fun, I. Razak and S. Dharmaprakash, *Acta Crystallographica Section E: Structure Reports Online*, 2006, 62, o896-o898.
64. P. S. Patil, J. B.-J. Teh, H.-K. Fun, I. A. Razak and S. M. Dharmaprakash, *Acta Crystallographica Section E*, 2006, 62, o1710-o1712.
65. L. H. D. N.B. Colthup, S.E. Wiberley Academic Press, New York, 1990.
66. G. Socrates, Wiley, New York, 1980.
67. W. G. F. F.R. Dollish, F.F. Bentley, , Wiley, New York, 1997.
68. B. C. Smith, *Infrared spectral interpretation: a systematic approach*, CRC press, 1998.
69. N. P. Roeges, *A guide to the complete interpretation of infrared spectra of organic structures*, Wiley, 1994.
70. G. Varsanyi, Academic Press, New York, 1969.
71. G. Varsányi, *Assignments for vibrational spectra of seven hundred benzene derivatives*, Halsted Press, 1974.
72. F. A. Miller, *Journal of Raman Spectroscopy*, 1988, 19, 219-221.
73. M. Gussoni and C. Castiglioni, *J. Mol. Struct.*, 2000, 521, 1-18.
74. D. Sajan, J. Binoy, I. Hubert Joe, V. S. Jayakumar and J. Zaleski, *Journal of Raman Spectroscopy*, 2005, 36, 221-236.
75. D. Sajan, I. H. Joe, J. Zaleski and V. S. Jayakumar, *Laser Physics Letters*, 2005, 2, 343-350.
76. C. Castiglioni, M. Del Zoppo and G. Zerbi, *Journal of Raman Spectroscopy*, 1993, 24, 485-494.
77. M. Tommasini, C. Castiglioni, M. Del Zoppo and G. Zerbi, *J. Mol. Struct.*, 1999, 480–481, 179-188.
78. D. Jacquemin, J. Preat and E. A. Perpète, *Chem. Phys. Lett.*, 2005, 410, 254-259.
79. D. Jacquemin, J. Preat, M. Charlot, V. Wathelet, J.-M. André and E. A. Perpète, *The Journal of chemical physics*, 2004, 121, 1736-1743.
80. M. Cossi and V. Barone, *The Journal of Chemical Physics*, 2001, 115, 4708-4717.
81. D. M. Bishop, *Adv. Quantum Chem.*, 1994, 25, 1-45.
82. P. N. Prasad and D. J. Williams, *Introduction to nonlinear optical effects in molecules and polymers*, Wiley New York etc., 1991.
83. V. E. Ingamells, M. G. Papadopoulos, N. C. Handy and A. Willetts, *The Journal of chemical physics*, 1998, 109, 1845-1859.
84. S. Raptis, M. G. Papadopoulos and A. Sadlej, *The Journal of chemical physics*, 1999, 111, 7904-7915.
85. U. Eckart, V. E. Ingamells, M. G. Papadopoulos and A. J. Sadlej, *The Journal of chemical physics*, 2001, 114, 735-745.

View Article Online
DOI: 10.1039/C5RA13494C

86. K. Govindarasu and E. Kavitha, *Spectrochimica Acta Part A: Molecular and Biomolecular Spectroscopy*, 2014, 122, 130-141.
87. C. Adant, M. Dupuis and J. Bredas, *Int. J. Quantum Chem*, 1995, 56, 497-507.
88. M. Karabacak and M. Cinar, *Spectrochimica Acta Part A: Molecular and Biomolecular Spectroscopy*, 2012, 86, 590-599.
89. R. Raju, C. Y. Panicker, P. S. Nayak, B. Narayana, B. Sarojini, C. Van Alsenoy and A. A. Al-Saadi, *Spectrochimica Acta Part A: Molecular and Biomolecular Spectroscopy*, 2015, 134, 63-72.
90. R. N. Singh, A. Kumar, R. K. Tiwari, P. Rawat, V. Baboo and D. Verma, *Spectrochimica Acta Part A: Molecular and Biomolecular Spectroscopy*, 2012, 92, 295-304.
91. K. Govindarasu and E. Kavitha, *Spectrochimica Acta Part A: Molecular and Biomolecular Spectroscopy*, 2014, 133, 799-810.
92. K. Govindarasu, E. Kavitha and N. Sundaraganesan, *Spectrochimica Acta Part A: Molecular and Biomolecular Spectroscopy*, 2014, 133, 417-431.
93. G. A. Babu and P. Ramasamy, *Mater. Chem. Phys.*, 2010, 119, 533-538.
94. A. Irfan, A. G. Al-Sehemi and M. S. Al-Assiri, *J. Fluorine Chem.*, 2014, 157, 52-57.
95. A. Irfan, A. G. Al-Sehemi and M. S. Al-Assiri, *Comp. Theor. Chem*, 2014, 1031, 76-82.
96. A. Irfan, *Optik - Intern. J. Light Elect. Optics*, 2014, 125, 4825-4830.
97. A. Vektariene, G. Vektaris and J. Svoboda, *Arkivoc*, 2009, 7, 311-329.
98. R. G. Pearson, *Journal of Chemical Education*, 1987, 64, 561.
99. J. S. Murray and K. Sen, *Molecular electrostatic potentials: concepts and applications*, Elsevier, 1996.
100. E. Scrocco and J. Tomasi, Academic Press, New York, 1978.